

Design and Research of a Bredigite Bone Repair Scaffold

Tingxin Liang¹, Fei Wang^{1*}, Jing Li¹, Yanbin Shi¹, Pengbo Liu¹, Shuaishuai Lu¹

¹School of Mechanical Engineering, Qilu University of Technology (Shandong Academy of Sciences),
China; Shandong Institute of Mechanical Design and Research, China

*Corresponding author: Fei Wang, School of Mechanical Engineering, Qilu University of Technology
(Shandong Academy of Sciences), China; Shandong Institute of Mechanical Design and Research,
China, e-mail address: wf@qlu.edu.cn

Submitted: 10th October 2024

Accepted: 9th January 2025

Abstract: *Purpose:* The fluid shear stress (FSS) generated by fluid flow after stent implantation is an important factor affecting the osteogenic ability of scaffolds and the proliferation and differentiation of osteoblasts are also affected by FSS. When the bone injury occurs, the blood flow at the defect changes from laminar flow to turbulent flow. Consequently, it is essential to employ a numerical simulation method that accurately reflects the actual conditions to study and analyze the surface FSS experienced by scaffolds and cells, thereby enhancing the osteogenic properties of the scaffolds. *Methods:* In this research, nine scaffolds with different structures and pore sizes were designed. The two-way fluid-structure interaction (FSI) method was used to evaluate scaffolds' internal flow field velocity and the surface FSS of scaffolds and cells. *Results:* The results show that the velocity distribution of different scaffolds is basically the same. FSS on the scaffold surface and FSS on cell surface decreased with the increase of scaffold aperture. FSS accepted by cells was much larger than that received by scaffolds, and FSS was distributed in a stepped pattern on the cell surface. *Conclusions:* Based on the FSS of the scaffold and cell surface, the triangle-600 and triangle-800 scaffolds have better osteogenic differentiation ability. This provides a more practical strategy for tissue engineering to design better scaffolds.

Keywords: Bone repair scaffold; Two-way FSI; Turbulence model; FSS

1. Introduction

With the develop at top speed of orthopedic treatment technology, the cure rate of bone defects has been increasing, but there are still some cases that cannot be cured due to various factors. Therefore, bone tissue engineering still faces many problems [24,44]. After the bone injury, the factors affecting bone healing include vascular dysfunction, insufficient osteoblast number, or decreased activity. These factors can make it difficult to form new bone in the injured area and hinder the natural healing process [27]. After bone tissue injury, its internal microenvironment will undergo certain changes, including a decrease in pH, a decrease in oxygen content, an increase in reactive oxygen species concentration, and so on [43]. According to relevant research, these factors will have certain adverse effects on bone injury repair [18]. Therefore, the creation of a microenvironment favorable for bone repair will facilitate the repair of bone defects [17].

A suitable 3D-printed bone repair scaffold is an important part of tissue engineering strategies [34]. Researching and developing bone-substituting biomaterials has attracted considerable interest in the biomaterials and orthopedics fields [32]. In addition to the selection of appropriate materials,

the macro- and microstructural properties of materials are crucial [54]. Ideal bone tissue engineering scaffolds suitable for bone defect treatment must have appropriate three-dimensional structure and porosity, be able to provide a high specific surface area for cell adhesion, have mechanical strength capable of carrying the bone defect site, and have biocompatibility, bone conductivity, bone induction, angiogenesis and biodegradability [13,33]. The porosity of 3D scaffolds for bone repair must be high enough and have a well-connected pore structure with a high specific surface area [16]. This will allow cells to grow inward and distribute throughout the porous scaffold, thus promoting the reconstruction and repair of bone tissue [14]. The scaffold shall also have sufficient micropores to facilitate the inward growth of capillaries. Porosity and pore connectivity are critical for the transport and exchange of nutrients and the elimination of metabolic wastes [22]. The pore size of the scaffold is also a matter of importance, because when it is too small, cells can clog the stent aperture. The proper pore size of the scaffold facilitates the formation of extracellular matrix and neovascularization. Scaffolds suitable for bone repair should have a pore size of 200-900 μm [15].

When a bone defect occurs, stem cells and bone tissue cells are recruited to the affected area and stimulated by physiological processes, which triggers their osteogenic differentiation [3]. However, when the size of the defect site is large, natural bone induction may not be sufficient [7]. Therefore, it is also required that the scaffold itself has a certain bone induction function to stimulate osteogenic differentiation in situ [2,21]. Materials used for scaffold preparation can generally be divided into polymers, bioceramics, and bioglass [30,47,48,49]. Polymers have attracted a lot of attention due to their high porosity, their biodegradability, their high specific surface area, and their mechanical stability [8].

Mechanical stimulation of osteoblasts in vivo involves bone matrix deformation and interstitial fluid flow; this is a highly valued method of mechanical stimulation of osteoblastic osteogenic differentiation of osteocytes [42,46]. ISF flows in response to mechanical loading, muscle contraction, blood pressure, and other influences, generating FSS at the cell surface [46]. A high degree of vascularisation is characteristic of bone tissue. When a bone defect occurs, a blood vessel is damaged by an external force and blood flows through the defect area as a result of the rupture [23,28]. FSS stimulates osteoblasts and osteocytes more significantly than other cells. When osteocytes are mechanically stimulated, osteoblasts can convert them into biochemical stimuli and rebuild bone tissue [12,42,52]. FSS can affect the expression, function and distribution of connexins

on the cell surface, as well as the synthesis, metabolism and release of growth factors, which in turn affect the biological behavior of cells [20]. Cell function and tissue growth can be predicted by taking control of the FSS [36]. Therefore, it is important to design suitable bone repair scaffolds and analyze cellular FSS to induce self-repair of bone tissue.

SALERNO et al. employed a FSS bioreactor to investigate the impacts of different ranges of FSS on scaffolds for bone repair [29]. Zhao et al. combination of CFD and FE to explore the effects of different scaffold structures on FSS [53]. D'Adamo et al. established a CFD model and found that there is higher shear stress near the entrance of the channel due to the development of the velocity profile [4]. In previous research, researchers have used a unidirectional fluid-solid coupling CFD method to study bone repair scaffolds, and have paid less attention to the impact of FSS on cells.

In previous research conducted by our group, a two-way fluid-structure interaction (FSI) model was established based on laminar flow [5]. However, during bone injury, damaged blood vessels rupture, resulting in a transition from laminar to turbulent flow [9]. In the early stages of bone repair, a turbulent bidirectional fluid-structure coupling model more accurately reflects the physiological conditions. Consequently, this study selected bredigite, known for its excellent biocompatibility and biosafety, as the scaffold material, established a turbulent two-way FSI model, and investigated the effects of fluid shear stress (FSS) on the scaffold and cells.

2. Materials and methods

2.1 Establishment of scaffold model and scaffold loaded cell model

This research used Solidworks 3D modeling software to model the scaffold model and established three types of scaffold models: square, cylinder, and right isosceles triangle. The scaffold structures were composed of square, cylinder, and right isosceles triangles, respectively. To meet the requirements of cell and ossification, each scaffold was established with three different scaffold sizes, namely different pore sizes, totaling nine types of scaffolds. According to different scaffold sizes and pore sizes, the models are named square 400-600-800 scaffold, cylinder 400-600-800 scaffold, and triangle 400-600-800 scaffold. For example, the triangle-400 scaffold represents a triangle structure with an aperture size of 400 μm . Table 1 shows the parameters of each scaffold model.

Table. 1 Parameter of each scaffold model

Structure	Square scaffold			Cylinder scaffold			Triangle scaffold		
Scaffold unit size (L , μm)	1000								
Aperture size (d , μm)	400	600	800	400	600	800	400	600	800

A hemisphere with a diameter of $19\mu\text{m}$ is the ideal cell model state [10,20]. Figure 1 reveals a cell model built using Solidworks In the experimental observation, there was a gap between each cell [51], so the position of the cell load on the scaffold required a certain symmetry, as shown in Figure 2. At the same time, the position of the cell load should be different to better reflect the FSS received by the cells inside the scaffold, taking into account the different flow velocities at each position inside the scaffold.

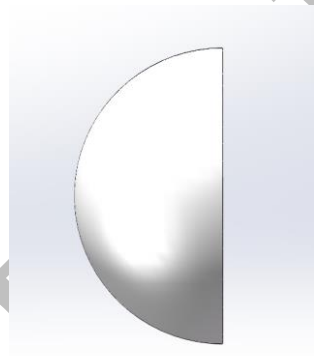


Figure. 1 Established cell models.

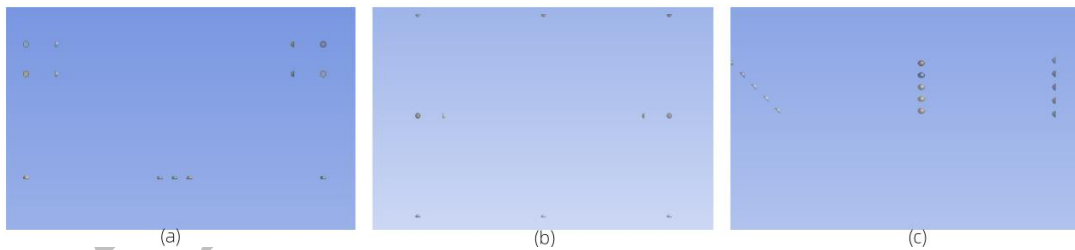


Figure. 2 Symmetrical distribution of loaded cells on the scaffold: (a) Square scaffold; (b) Cylinder scaffold; (c) Triangle scaffold.

2.2 Two-way FSI flow path

The established two-way FSI model created splits the whole into two parts, the fluid domain and the solid domain (Figure 1 (d)), with the fluid domain being the blood flow region and the solid domain being the scaffold and cells. The two-way FSI model places the fluid domain on a solid surface subjected to fluid impact stresses, where the solid domain will deform and change the area of the fluid domain as a result of the forces transmitted by the fluid domain. The surface on which

force and displacement are transferred is the FSI surface, which will be placed at the surface in contact between the fluid and the solid. This research selected the scaffold surface and cell surface as the FSI surface. Cells loaded with square scaffold and triangle scaffold are $5 \times 5 \times 5$ units, and cylinder scaffold loaded with $4 \times 4 \times 4$ units. The middle region of the scaffold model has less fluid velocity dispersion, so when the fluid passes through this region, its velocity will be higher than when it passes through other locations of the scaffold. When the surface of the cell loaded on the scaffold has fluid passing over it, the force and the resulting deformation of the cell under the impact of the fluid are larger, and the maximum result of the whole scaffold model can be approximated by the FSS and deformation of the cell surface here. Therefore, the cell load is located in the middle of the scaffold, as shown in Figure 2 (d).

2.3 Boundary condition

The scaffold material is selected as bredigite, with an elastic modulus of 118GPa and a Poisson's ratio of 0.3. The elastic modulus of cells is 4470Pa, and the Poisson's ratio is 0.4 [38,41,52]. Due to the rupture of blood vessels after bone damage, the fluid medium in the fluid domain is set as blood, with a density of 1060 kg/m³ and a viscosity of 0.003 kg/s [6,35]. Model inlet velocity is set to 0.1 mm/s [43,44], the wall of the fluid domain is set as a non-slip boundary and the pressure at the outlet is set to 0 Pa, as shown in Figure 3. Set the flow model to a turbulence model.

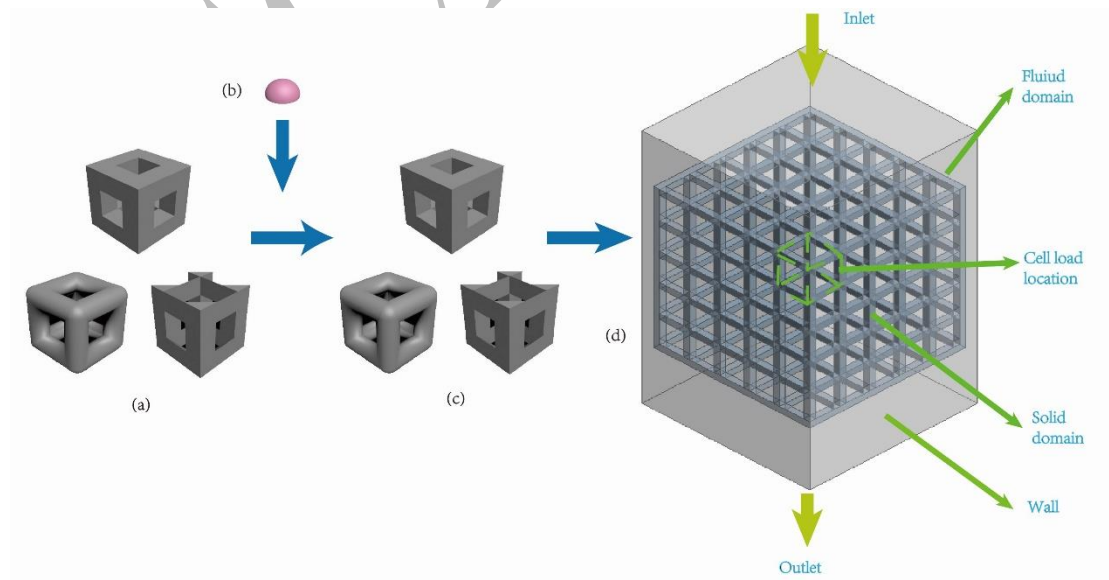


Figure 3 Two-way FSI flow chart: (a) Scaffold unit: square scaffold on the top, cylinder scaffold on the lower left, triangle scaffold on the lower right; (b) Cells loaded onto the scaffold; (c) Scaffold unit after the loaded cell: square scaffold at the top, cylinder scaffold at the lower left, and triangle scaffold at the lower right; (d) The two-

way FSI model was established: the scaffold and cells are set up as solid domains, the blood was in the fluid domain, and the middle position of the scaffold is the loaded cells.

2.4 Governing equation

Two-way fluid-structure interaction follows the most basic conservation principle, and at the FSI interface of fluid-structure coupling, the fluid-structure stress should be satisfied (τ). The equality or conservation of displacement (d) variables satisfies the following two equations:

$$\begin{cases} \tau_f \cdot n_f = \tau_s \cdot n_s \\ d_f = d_s \end{cases} \quad (1)$$

FSS is calculated by the following equation:

$$\tau = \mu \frac{\partial v}{\partial n} \quad (2)$$

In the equation, v and μ represent velocity (m/s) and dynamic viscosity (kg/m/s) respectively, and velocity (m/s), n represents the x -, y -, and z - directions of the coordinate axis.

The Reynolds number is calculated by the following formula:

$$Re = \frac{\rho v D}{\mu} \quad (3)$$

In the equal, ρ , μ , D , and v are fluid density (kg/m³), dynamic viscosity (kg/m/s), pore hydrodynamic diameter (m), and inlet velocity (m/s).

2.5 Solution

Perform two-way fluid-structure interaction analysis using the Fluent and Transient structure modules in Ansys software to obtain the flow velocity of the scaffold and the scaffold surface FSS as well as the cell surface FSS.

3. Result

3.1 Flow field analysis

The flow rates of the 9 scaffolds are shown in Figure 4, and the size of FSS received by cells (Figure 7) is positively correlated with fluid velocity. The flow velocity distribution of the three scaffold structures is basically the same. When the fluid begins to enter the interior of the scaffold, the decrease in the entrance area of the scaffold cell leads to a sharp add in flow velocity. Moreover, the surface area of contact with the fluid at the entrance of the cell is large, and the cells in this area are subjected to the largest FSS. When the fluid flows inside the scaffold, the area and pores inside the scaffold increase, and the fluid disperses around, resulting in a slower flow rate. When the pore diameter of the scaffold gradually becomes larger, the flow of fluid through the scaffold will be

dispersed faster, and the velocity of the fluid will be reduced. The cell surface FSS also decreased with the increase of the contact area of the fluid with the inner surface of the scaffolds. At this time, it is very favorable for cells to deposit, adhere, and proliferate inside the scaffold.

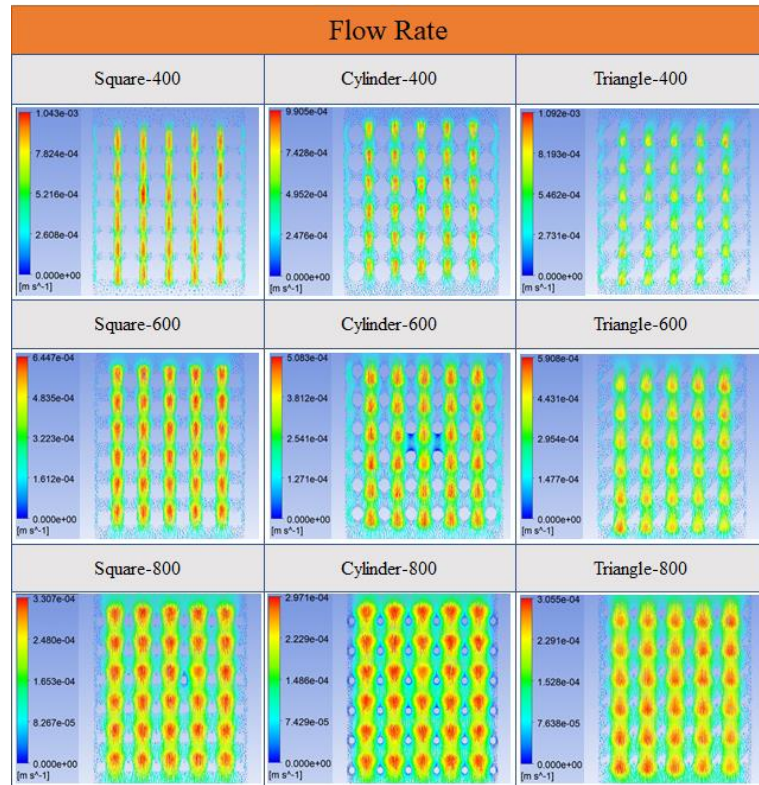


Figure. 4 Flow rate distribution of the scaffold in the flow field.

3.2 Scaffold surface FSS analysis

Bone tissue engineering expects to design bone repair scaffolds with excellent osteogenic capacity, which can be predicted by quantitative analysis of the FSS to which the scaffold surface is subjected. The ANSYS Fluent module can calculate the FSS size of bone repair scaffold models in fluid flow, and the distribution of the FSS for each of the scaffold models is shown in Figure 5. The surface of the maximum FSS received by each scaffold model is located at the direct contact point of the fluid, that is, at the inlet and outlet of each scaffold unit model. This is also verified by the aforementioned fluid velocity magnitude (Figure 4). The surface FSS of each scaffold model decreases with increasing scaffold aperture, but the osteogenic properties could not be directly assessed. Osteogenic differentiation was favored when the FSS was <30 mPa. From Figure 6, we can see the percentage of the surface of each scaffold that was subjected to FSS <30 mPa, which is the percentage of scaffolds that were able to complete osteogenic differentiation.

Figure 6 highlights that when the pore size of the scaffold increases, the area of the scaffold

surface that is favorable for cells to undergo osteogenic differentiation increases with it. When the aperture of the scaffold is $400\mu\text{m}$, the area of $\text{FSS} < 30\text{mPa}$ on all three scaffolds is above 93%, which is well suited for the osteogenic differentiation on the scaffold surface. When the aperture of the scaffold is $600\mu\text{m}$ and $800\mu\text{m}$, the area of $\text{FSS} < 30\text{mPa}$ on all three scaffolds is 100%, which is beneficial for osteogenic differentiation on the surface of the scaffold. Under different pore sizes, the area of the triangle scaffold subjected to $\text{FSS} < 30\text{mPa}$ is close to or equal to 100%, which also means that the triangle scaffold has the strongest osteogenic differentiation ability.

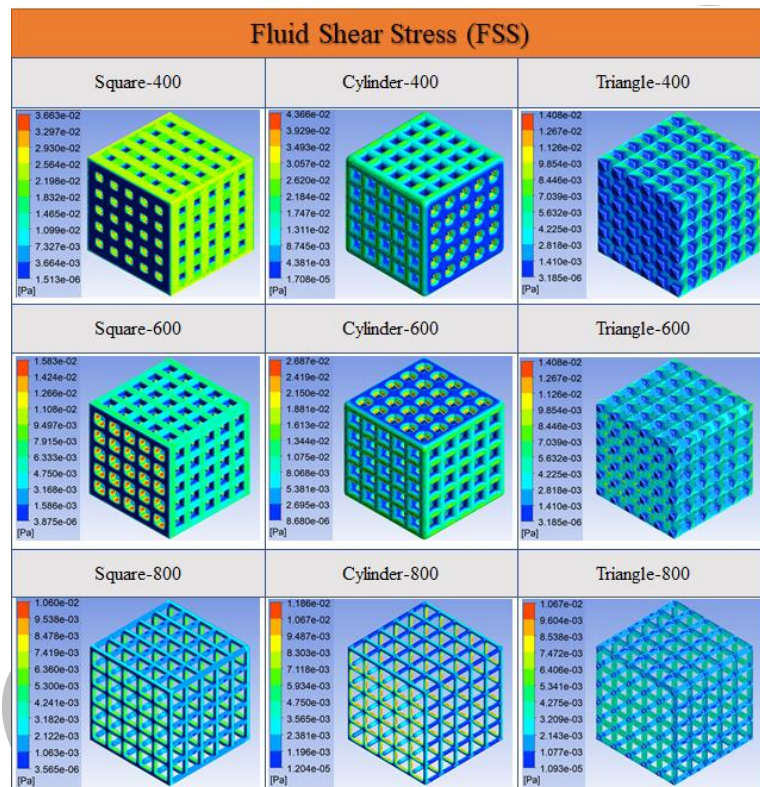


Figure. 5 Distribution of FSS to which the surface of the scaffold is subjected.

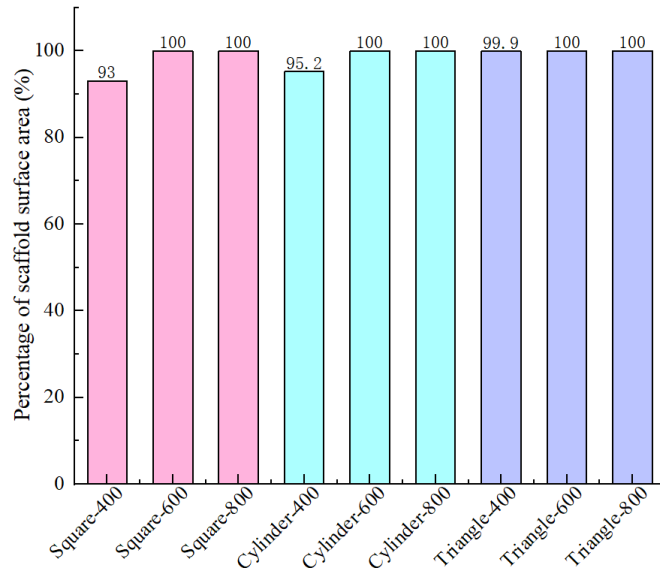


Figure. 6 The percentage of osteogenic differentiation on the scaffold surface, that is, the proportion of the area with FSS<30mPa.

3.3 Cell surface FSS analysis

The surface FSS to which the cells are subjected is also important for osteogenic differentiation, and this part of the effect has often been overlooked in previous research. Cells attached to the surface of the scaffold are of a certain height, and the height of the protrusion causes the cell surface to be subjected to a greater fluid action, producing a greater FSS relative to the surface of the scaffold. Figure 6 illustrates the distribution of surface FSS to which the cell is subjected to fluid action, while Table 2 shows the amount of deformation produced by the cell due to fluid action. The presence of cell surface height also affects the distribution position of FSS on the cell surface, and when the cell surface height increases, the cell surface FSS increases subsequently. The amount of cell deformation and fluid velocity are positively correlated with the surface FSS to which the cell is subjected. Table 2, Figure 4, and Figure 7 can be mutually verified.

Table. 2 The amount of deformation that occurs in cells loaded onto different scaffolds.

	Cell deformation (mm)
Square-400	3.3857e-007
Square-600	1.0955e-007
Square-800	6.334e-008
Cylinder-400	2.3772e-007
Cylinder-600	9.4033e-008
Cylinder-800	7.2645e-008

Triangle-400	1.3274e-007
Triangle-600	6.8225e-008
Triangle-800	6.806e-008

Figure 7 illustrates the top of the cell is subjected to a huge difference in FSS compared to the bottom, and the closer to the top of the cell, the larger the FSS, which indicates that the FSS subjected to the surface of the scaffold cannot replace the cell. At the same time, the FSS to which the cells were subjected was also correlated with the location of the cells inside the scaffold, with cells in the direction of fluid flow being subjected to a larger FSS due to direct contact with the fluid, and cells closer to the center of the fluid being subjected to a larger FSS. The overall FSS to which the cell surface is subjected is distributed in a stepwise manner.

The percentage of cell surface FSS is shown in Figure 8. The FSS to which the cells were subjected gradually decreased and the number of cells capable of osteogenic differentiation increased as the aperture size of the scaffold increased. The FSS to which the cells inside the square-400 and cylinder-400 scaffolds were subjected was larger, and a larger area was not suitable for osteogenic differentiation. The remaining scaffold internal cells were subjected to FSS <30 mPa in a percentage of surface area close to or equal to 100%, indicating that they were suitable for osteogenic differentiation. The percentage of surface area of the inner cells of the triangle-400 scaffold subjected to FSS <30 mPa was 98.5%, whereas the percentage of surface area of the inner cells of the triangle-600 scaffold and triangle-800 scaffold subjected to FSS <30 mPa was 100%.

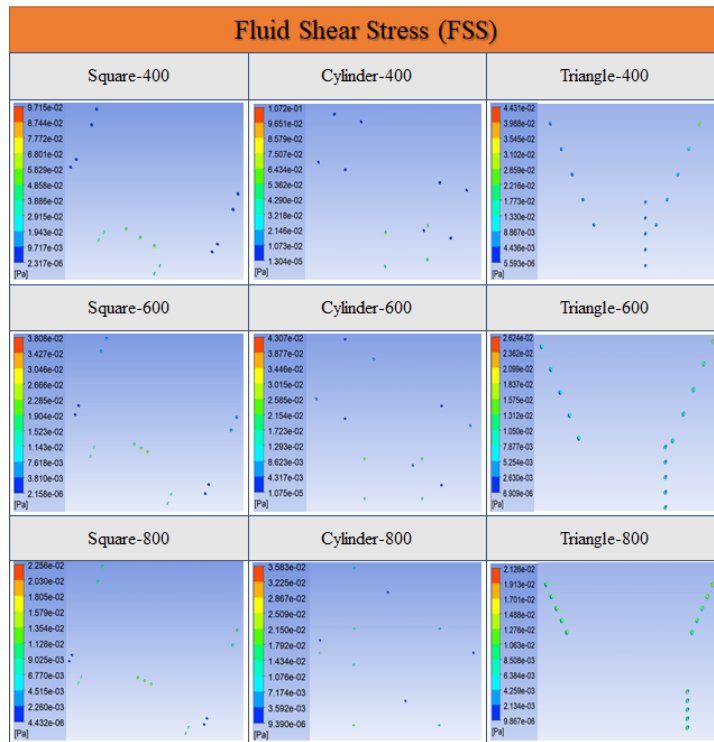


Figure. 7 Distribution of FSS applied to the surface of cells loaded onto the scaffolds.

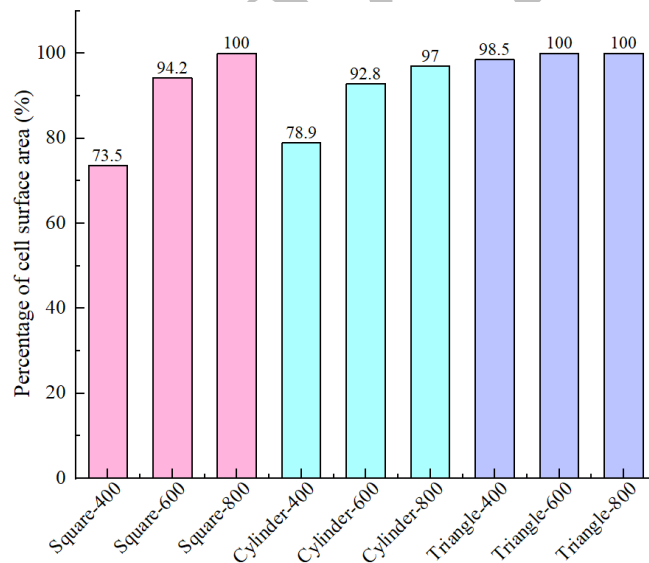


Figure. 8 The percentage of osteogenic differentiation on the cell surface, that is, the proportion of the area with $FSS < 30 \text{ mPa}$.

Differential analysis of the area percentage of cell surface $FSS < 30 \text{ mPa}$ was performed using the AVONA method in SPSS software to investigate the effect of different scaffold structures on the scaffold osteogenic performance. The results are shown in Figure 8, the mean values of the area percentage of cell $FSS < 30 \text{ mPa}$ for square scaffolds, cylinder scaffolds, and triangle scaffolds were 89.2%, 89.6%, and 99.5%, respectively, and the standard deviations were 13.9%, 9.5%, and 0.8%,

respectively. The error standard deviation gradually increased for square scaffolds, cylinder scaffolds and triangle scaffolds. There was no significant difference between square scaffolds and cylinder scaffolds, while there was a significant difference between triangle scaffolds and square and cylinder scaffolds. In conclusion, the triangle structure of the scaffolds had superior osteogenic properties.

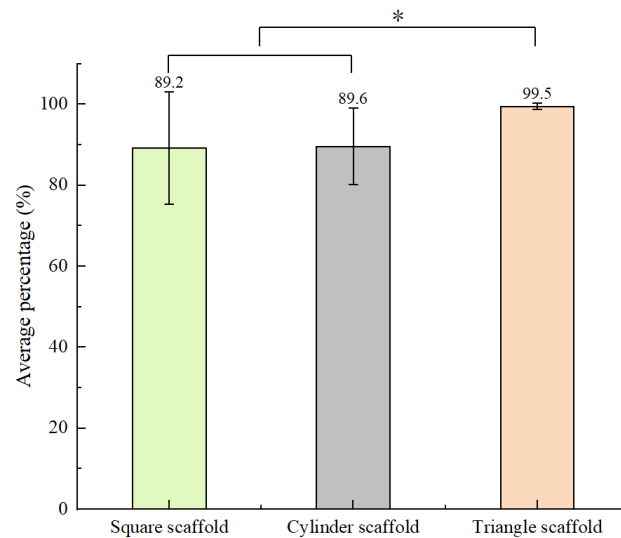


Figure. 9 Statistical analysis of square scaffolds, cylinder scaffolds and triangle scaffold.

4. Discussion

Porous scaffolds have become the focus of tissue engineering research because of their good osteogenic properties. In this research, three different scaffold structures were designed, and each scaffold was subdivided into three different pore sizes based on the pore size, totaling nine scaffold structures. The flow velocity and surface FSS of the scaffolds in the flow field as well as the cell surface FSS were investigated by using a two-way FSI method.

Blood is responsible for transporting nutrients such as oxygen, glucose and metabolites in the body, and the transport rate of nutrients and metabolites is an important factor affecting bone regeneration [25,39]. The distribution of fluid flow field in the scaffold has an important effect on the transport rate. The internal flow velocity of the nine scaffolds was the same, and the flow velocity increased dramatically when the fluid started to enter the inside of the scaffolds. As the fluid flowed inside the scaffolds, the internal area and pores of the scaffolds increased, the fluid dispersed in all directions, and the flow rate slowed down. As the pore size of each stent becomes larger, the fluid gets dispersed rapidly, the velocity of the fluid through the scaffold becomes smaller, and the FSS

to which the cells are subjected becomes smaller. This situation is in favour of cell deposition, adhesion, and proliferation, which is suitable for osteogenic differentiation.

The fluid shear stress caused by ISF flow can stimulate osteoblast differentiation [8,42,46]. Some in vitro experimental studies have confirmed the above point [11,45]. Therefore, FSS is an important index to evaluate the osteogenic performance of scaffolds. When the $FSS < 30 \text{ mPa}$, the scaffold will be conducive to osteogenic differentiation of the defect [26,31,37,52]. FSS can not be accurately measured under actual in vivo conditions, but FSS can be accurately predicted with the help of numerical simulation software. How to accurately simulate human environment in numerical simulation software is a hot research topic at present. In previous studies, researchers often set the blood flow form as laminar flow [5]. But when the bone injury occurs, the damaged blood vessels rupture, and the blood flow changes from laminar flow to turbulent flow [9]. In the preliminary stage of bone repair, the two-way FSI model based on turbulence is more consistent with the real situation.

The FSS of 9 kinds of scaffolds increases with the decrease of the aperture of scaffolds, the area of the scaffold surface suitable for osteogenic differentiation also increases, which means that the osteogenic differentiation capacity of each structural scaffold is subsequently enhanced. It also corresponds to previous studies [50]. The surface FSS to which the cells are subjected is also important for osteogenic differentiation, and this part of the effect has often been neglected in previous studies [19,50,53]. Loading cells into the middle of the scaffold approximates the maximum FSS of osteoblasts attached to the scaffold after implantation in vivo. The FSS on the cell surface of each scaffold was consistent with the FSS on the scaffold surface, that is, the FSS decreased with the increase of the pore size and was more conducive to osteogenic differentiation. The FSS on the cell surface is much larger than the scaffold. This is because cells adhering to the scaffold surface are of a certain height, and the height of the protrusion causes the cell surface to be subjected to a greater fluid action, generating a greater FSS relative to the scaffold surface. Compared with the previous design of our research group, the osteogenic performance has been improved [5]. Different scaffold structures have significant effects on the osteogenic performance of scaffolds. The difference analysis of osteogenic properties of different scaffolds by statistics showed that compared with square scaffolds and cylinder scaffolds, triangle scaffolds had better osteogenic ability.

Compared with previous studies, the scaffolds designed by this numerical simulation method perform better. Triangle scaffolds were superior to square and cylindrical scaffolds in both FSS on scaffold surface and FSS on cell surface, so triangle scaffolds would be a more favorable choice for bone repair.

5. Conclusions

In this research, nine bone repair scaffolds with different structures and aperture sizes were designed and loaded with different locations and numbers of cells depending on the scaffold structure. The fluid flow inside the scaffolds was analyzed with the help of two-way fluid-structure interaction in ANSYS software. The flow velocity and surface FSS inside the scaffolds as well as the cell surface FSS were investigated. The results of this research as well as the innovative models are shown below:

1. The turbulence model was selected for analysis as it aligns more closely with the actual conditions of human bone defects.
2. The two-way fluid-structure interaction (FSI) model was developed to analyze the surface fluid shear stress (FSS) experienced by the cells within the scaffold. This model takes into account cell deformation and provides an accurate assessment of the surface FSS acting on the cells.
3. The flow rate of all scaffold models is conducive to the transport of nutrients and metabolites.
4. Both scaffold FSS and cell FSS decreased with the increase of scaffold aperture
5. Statistical analysis showed that different scaffold structures had significant effects on the osteogenic performance of scaffolds
6. Triangle scaffolds perform well in both scaffold FSS and cell FSS. Among them, triangle-600 and triangle-800 are suitable scaffold structures for bone repair.

Acknowledgments

This work was supported by the Shandong Key R&D Program (Major Scientific and Technological Innovation Project) (NO. 2024CXGC010208) and Natural Science Foundation project of Shandong Province (NO. ZR2022ME086).

Reference

- [1] Ali D, Sen S. Finite element analysis of mechanical behavior, permeability and fluid induced wall shear stress of high porosity scaffolds with gyroid and lattice-based architectures, *Journal of the mechanical behavior of biomedical materials*, 2017, 75: 262-270, DOI: 10.1016/j.jmbbm.2017.07.035.
- [2] Bohner M, Miron R J. A proposed mechanism for material-induced heterotopic ossification, *Materials Today*,

- 2019, 22: 132-141, DOI; 10.1016/j.mattod.2018.10.036.
- [3] Bose S, Fielding G, Tarafder S, et al. Understanding of dopant-induced osteogenesis and angiogenesis in calcium phosphate ceramics. *Trends in biotechnology*, 2013, 31(10): 594-605, DOI: 10.1016/j.tibtech.2013.06.005.
- [4] D'ADAMO, Alessandro, et al. Experimental measurements and CFD modelling of hydroxyapatite scaffolds in perfusion bioreactors for bone regeneration. *Regenerative Biomaterials*, 2023, 10: rbad002, DOI:10.1093/rb/rbad002.
- [5] Fu M, Wang F, Lin G. Design and research of bone repair scaffold based on two-way fluid-structure interaction, *Computer Methods and Programs in Biomedicine*, 2021, 204: 106055, DOI: 10.1016/j.cmpb.2021.106055.
- [6] Gao Y, Shi Y, Fu M, et al, Simulation study of the effects of interstitial fluid pressure and blood flow velocity on transvascular transport of nanoparticles in tumor microenvironment, *Computer Methods and Programs in Biomedicine*, 2020, 193: 105493, DOI: 10.1016/j.cmpb.2020.105493.
- [7] Geiger F, Bertram H, Berger I, et al. Vascular endothelial growth factor gene-activated matrix (VEGF165-GAM) enhances osteogenesis and angiogenesis in large segmental bone defects, *Journal of Bone and Mineral Research*, 2005, 20(11): 2028-2035, DOI: 10.1359/JBMR.050701.
- [8] Guvendiren M, Molde J, Soares R M D, et al. Designing biomaterials for 3D printing, *ACS biomaterials science & engineering*, 2016, 2(10): 1679-1693, DOI: 10.1021/acsbiomaterials.6b00121.
- [9] JIA, Mengping, et al. Deletion of BACH1 attenuates atherosclerosis by reducing endothelial inflammation, *Circulation Research*, 2022, 130(7): 1038-1055, DOI: 10.1161/CIRCRESAHA.121.319540.
- [10] Jungreuthmayer C, Jaasma M J, Al-Munajjed A A, et al. Deformation simulation of cells seeded on a collagen-GAG scaffold in a flow perfusion bioreactor using a sequential 3D CFD-elastostatics model, *Medical engineering & physics*, 2009, 31(4): 420-427, DOI: 10.1016/j.medengphy.2008.11.003.
- [11] Kapur S, Baylink DJ, Lau KHW. Fluid flow shear stress stimulates human osteoblast proliferation and differentiation through multiple interacting and competing signal transduction pathways, *Bone*. 2003; 32(3): 241-251, DOI: 10.1016/S8756-3282(02)00979-1.
- [12] Kim M S, Lee M H, Kwon B J, et al. Enhancement of human mesenchymal stem cell infiltration into the electrospun poly (lactic-co-glycolic acid) scaffold by fluid shear stress, *Biochemical and Biophysical Research Communications*, 2015, 463(1-2): 137-142, DOI: 10.1016/j.bbrc.2015.05.048.
- [13] Koons G L, Diba M, Mikos A G. Materials design for bone-tissue engineering, *Nature Reviews Materials*, 2020, 5(8): 584-603, DOI: 10.1038/s41578-020-0204-2.
- [14] Kopp A, Derra T, Müther M, et al. Influence of design and postprocessing parameters on the degradation behavior and mechanical properties of additively manufactured magnesium scaffolds, *Acta biomaterialia*, 2019, 98: 23-35, DOI: 10.1016/j.actbio.2019.04.012.
- [15] Lai Y, Cao H, Wang X, et al. Porous composite scaffold incorporating osteogenic phytomolecule icariin for promoting skeletal regeneration in challenging osteonecrotic bone in rabbits, *Biomaterials*, 2018, 153: 1-13, DOI: 10.1016/j.biomaterials.2017.10.025.
- [16] Lai Y, Li Y, Cao H, et al. Osteogenic magnesium incorporated into PLGA/TCP porous scaffold by 3D printing for repairing challenging bone defect, *Biomaterials*, 2019, 197: 207-219, DOI: 10.1016/j.biomaterials.2019.01.013.
- [17] Li H, Wang H, Pan J, et al. Nanoscaled Bionic Periosteum Orchestrating the Osteogenic Microenvironment for Sequential Bone Regeneration, *ACS Appl Mater Interfaces*, 2020, 12(33): 36823-36, DOI: 10.1021/acsami.0c06906.
- [18] Li Y, Pan Q, Xu J, et al. Overview of methods for enhancing bone regeneration in distraction osteogenesis: Potential roles of biomaterials, *Journal of orthopaedic translation*, 2021, 27: 110-118, DOI: 10.1016/j.jot.2020.11.008.
- [19] Liu L, Wang S, Liu J, et al. Architectural design of Ti6Al4V scaffold controls the osteogenic volume and application area of the scaffold, *Journal of Materials Research and Technology*, 2020, 9(6): 15849-15861, DOI: 10.1016/j.jmrt.2020.11.061.
- [20] Ma C, Du T, Niu X, et al. Biomechanics and mechanobiology of the bone matrix, *Bone research*, 2022, 10(1):

59, DOI: 10.1038/s41413-022-00223-y.

[21]Meng J, Xiao B, Zhang Y, et al. Super-paramagnetic responsive nanofibrous scaffolds under static magnetic field enhance osteogenesis for bone repair in vivo, *Scientific reports*, 2013, 3(1): 2655, DOI: 10.1038/srep02655.

[22]Mercado-Pagán Á E, Stahl A M, Shanjani Y, et al. Vascularization in bone tissue engineering constructs, *Annals of Biomedical Engineering*, 2015, 43(3): 718-729, DOI: 10.1007/s10439-015-1253-3.

[23]Milan J L, Planell J A, Lacroix D. Computational modelling of the mechanical environment of osteogenesis within a polylactic acid–calcium phosphate glass scaffold, *Biomaterials*, 2009, 30(25): 4219-4226, DOI: 10.1016/j.biomaterials.2009.04.026.

[24]Nabiyouni M, Brückner T, Zhou H, et al. Magnesium-based bioceramics in orthopedic applications, *Acta biomaterialia*, 2018, 66: 23-43, DOI: 10.1016/j.actbio.2017.11.033.

[25]Nambiar J, Jana S, Nandi S K. Strategies for Enhancing Vascularization of Biomaterial-Based Scaffold in Bone Regeneration, *The Chemical Record*, 2022, 22(6): e202200008, DOI: 10.1002/tcr.202200008.

[26]Olivares A L, Marsal È, Planell J A, et al. Finite element study of scaffold architecture design and culture conditions for tissue engineering, *Biomaterials*, 2009, 30(30): 6142-6149, DOI: 10.1016/j.biomaterials.2009.07.041.

[27]Ossendorf C, Kaps C, Kreuz P C, et al. Treatment of posttraumatic and focal osteoarthritic cartilage defects of the knee with autologous polymer-based three-dimensional chondrocyte grafts: 2-year clinical results, *Arthritis research & therapy*, 2007, 9: 1-11, DOI: 10.1186/ar2180.

[28]Ouyang P, Dong H, He X, et al. Hydromechanical mechanism behind the effect of pore size of porous titanium scaffolds on osteoblast response and bone ingrowth, *Materials & Design*, 2019, 183: 108151, DOI:10.1016/j.matdes.2019.108151.

[29]Salerno E, Orlandi G, Ongaro C, et al. Liquid flow in scaffold derived from natural source: experimental observations and biological outcome, *Regenerative Biomaterials*, 2022, 9: rbac034, DOI: 10.1093/rb/rbac034.

[30]Salgado A J, Coutinho O P, Reis R L. Bone tissue engineering: state of the art and future trends, *Macromolecular bioscience*, 2004, 4(8): 743-765, DOI: 10.1002/mabi.200400026.

[31]Sandino C, Lacroix D. A dynamical study of the mechanical stimuli and tissue differentiation within a CaP scaffold based on micro-CT finite element models, *Biomechanics and modeling in mechanobiology*, 2011, 10: 565-576, DOI: 10.1007/s10237-010-0256-0.

[32]Schatkoski V M, Larissa do Amaral Montanheiro T, Canuto de Menezes B R, et al. Current advances concerning the most cited metal ions doped bioceramics and silicate-based bioactive glasses for bone tissue engineering, *Ceramics International*, 2021, 47(3): 2999-3012, DOI: 10.1016/j.ceramint.2020.09.213.

[33]Shuai C, Yang W, He C, et al. A magnetic micro-environment in scaffolds for stimulating bone regeneration, *Materials & Design*, 2020, 185: 108275, DOI: 10.1016/j.matdes.2019.108275.

[34]Sinha R, Camara-Torres M, Scopece P, et al. A hybrid additive manufacturing platform to create bulk and surface composition gradients on scaffolds for tissue regeneration, *Nat Commun*, 2021, 12(1): 500, DOI: 10.1038/s41467-020-20865-y.

[35]Sohrabi S, Zheng J, Finol E A, et al. Numerical simulation of particle transport and deposition in the pulmonary vasculature, *Journal of biomechanical engineering*, 2014, 136(12): 121010, DOI:10.1115/1.4028800.

[36]Stops A J F, Heraty K B, Browne M, et al. A prediction of cell differentiation and proliferation within a collagen–glycosaminoglycan scaffold subjected to mechanical strain and perfusive fluid flow[J]. *Journal of biomechanics*, 2010, 43(4): 618-626, DOI: 10.1016/j.jbiomech.2009.10.037.

[37]Stops A J F, Heraty K B, Browne M, et al. A prediction of cell differentiation and proliferation within a collagen–glycosaminoglycan scaffold subjected to mechanical strain and perfusive fluid flow, *Journal of biomechanics*, 2010, 43(4): 618-626, DOI: 10.1016/j.jbiomech.2009.10.037.

[38]Sugawara Y, Ando R, Kamioka H, et al. The alteration of a mechanical property of bone cells during the process

- of changing from osteoblasts to osteocytes, *Bone*, 2008, 43(1): 19-24, DOI: 10.1016/j.bone. 2008.02.020.
- [39] Tomlinson R E, Silva M J. Skeletal blood flow in bone repair and maintenance, *Bone research*, 2013, 1(1): 311-322, DOI: 10.4248/BR201304002.
- [40] Truscello S, Kerckhofs G, Van Bael S, et al. Prediction of permeability of regular scaffolds for skeletal tissue engineering: a combined computational and experimental study, *Acta biomaterialia*, 2012, 8(4): 1648-1658, DOI: 10.1016/j.actbio.2011.12.021.
- [41] Vaughan T J, Haugh M G, McNamara L M. A fluid–structure interaction model to characterize bone cell stimulation in parallel-plate flow chamber systems, *Journal of The Royal Society Interface*, 2013, 10(81): 20120900, DOI:10.1098/rsif.2012.0900.
- [42] Verbruggen S W, Vaughan T J, McNamara L M. Fluid flow in the osteocyte mechanical environment: a fluid–structure interaction approach, *Biomechanics and modeling in mechanobiology*, 2014, 13(1): 85-97, DOI:10.1007/s10237-013-0487-y.
- [43] Walters G, Pountos I, Giannoudis P V. The cytokines and micro-environment of fracture haematoma: Current evidence, *Journal of tissue engineering and regenerative medicine*, 2018, 12(3): e1662-e1677, DOI: 10.1002/term.2593.
- [44] Wang S J, Jiang D, Zhang Z Z, et al. Biomimetic nano silica–collagen scaffolds for in situ bone regeneration: toward a cell-free, one-step surgery, *Advanced Materials*, 2019, 31(49): 1904341, DOI: 10.1002/adma.201904341.
- [45] Weinbaum S, Cowin S C, Zeng Y. A model for the excitation of osteocytes by mechanical loading-induced bone fluid shear stresses, *Journal of biomechanics*, 1994, 27(3): 339-360, DOI:10.1016/0021-9290(94)90010-8.
- [46] Wittkowske C, Reilly G C, Lacroix D, et al. In vitro bone cell models: impact of fluid shear stress on bone formation, *Frontiers in bioengineering and biotechnology*, 2016, 4: 87, DOI:10.3389/fbioe.2016.00087.
- [47] Wu C, Ramaswamy Y, Zhu Y, et al. The effect of mesoporous bioactive glass on the physiochemical, biological and drug-release properties of poly (DL-lactide-co-glycolide) films, *Biomaterials*, 2009, 30(12): 2199-2208, DOI: 10.1016/j.biomaterials.2009.01.029.
- [48] Wu Y, Jiang W, Wen X, et al. A novel calcium phosphate ceramic–magnetic nanoparticle composite as a potential bone substitute, *Biomedical Materials*, 2010, 5(1): 015001, DOI: 10.1088/1748-6041/5/1/015001.
- [49] Yoon J J, Kim J H, Park T G. Dexamethasone-releasing biodegradable polymer scaffolds fabricated by a gas-foaming/salt-leaching method, *Biomaterials*, 2003, 24(13): 2323-2329, DOI: 10.1016/S0142-9612(03)00024-3.
- [50] Zamani Y, Amoabediny G, Mohammadi J, et al. 3D-printed poly (ϵ -caprolactone) scaffold with gradient mechanical properties according to force distribution in the mandible for mandibular bone tissue engineering, *Journal of the mechanical behavior of biomedical materials*, 2020, 104: 103638, DOI: 10.1016/j.jmbbm.2020.103638.
- [51] Zhao D W, Zuo K Q, Wang K, et al. Interleukin-4 assisted calcium-strontium-zinc-phosphate coating induces controllable macrophage polarization and promotes osseointegration on titanium implant, *Materials Science and Engineering: C*, 2021, 118: 111512, DOI:10.1016/j. msec.2020.111512.
- [52] Zhao F, Vaughan T J, Mcnamara L M. Multiscale fluid–structure interaction modelling to determine the mechanical stimulation of bone cells in a tissue engineered scaffold, *Biomechanics and modeling in mechanobiology*, 2015, 14: 231-243, DOI:10.1007/s10237-014-0599-z.
- [53] Zhao F, Vaughan T J, McNamara L M. Quantification of fluid shear stress in bone tissue engineering scaffolds with spherical and cubical pore architectures, *Biomechanics and modeling in mechanobiology*, 2016, 15: 561-577, DOI: 10.1007/s10237-015-0710-0.
- [54] Zhu L, Luo D, Liu Y. Effect of the nano/microscale structure of biomaterial scaffolds on bone regeneration, *International Journal of Oral Science*, 2020, 12(1): 6, DOI: 10.1038/s41368-020-0073-y.